Sensors and Materials, Vol. 34, No. 12 (2022) 4325–4338
MYU Tokyo

S & M 3113

Method of Water Body Information Extraction in Complex Geographical Environment from Remote Sensing Images

Chao Chen,[1,2,3] Jintao Liang,[1] Zhisong Liu,[4,5] Wenxue Xu,[6*]
Zili Zhang,[7] Xin Zhang,[2] and Jianyu Chen[3]

[1]Marine Science and Technology College, Zhejiang Ocean University, Zhoushan 316022, China
[2]State Key Laboratory of Remote Sensing Science, Aerospace Information Research Institute, Chinese Academy of Sciences, Beijing 100101, China
[3]State Key Laboratory of Satellite Ocean Environment Dynamics, Second Institute of Oceanography, Ministry of Natural Resources, Hangzhou 310012, China
[4]Key Laboratory of Oceanographic Big Data Mining and Application of Zhejiang Province, Zhoushan 316022, China
[5]School of Information Engineering, Zhejiang Ocean University, Zhoushan 316022, China
[6]First Institute of Oceanography, Ministry of Natural Resources, Qingdao 266061, China
[7]Zhejiang Province Ecological Environment Monitoring Center (Zhejiang Key Laboratory of Ecological and Environmental Monitoring, Forewarning and Quality Control), Hangzhou 310012, China

(Received August 2, 2022; accepted November 22, 2022)

Keywords: water body information extraction, remote sensing imagery, tasseled cap transformation, complex geographical environment, accuracy assessment

The water body on the earth's surface is an important element of the environmental ecosystem. Floating matter, suspended matter, and dissolved matter negatively affect most traditional methods used to extract water body information from remotely sensed images. As a result, extracting water body information with high precision from a wide range from remote sensing images that contain complex ground-based objects has proved difficult. In this study, we proposed a method of extracting water body information from a remote sensing image that considers the wetness of ground-based objects, and we carried out threshold value selection using the Otsu method and post-processing supported by mathematical morphology. Hangzhou Bay, which is rich in inland water resources and marine resources, was selected as the study area. The results obtained from a Landsat 8 Operational Land Imager (OLI) image show that the contours and spatial extent of the water extracted by the method are highly consistent, with reduced effects of floating matter, suspended matter, and dissolved matter; the producer's accuracy and user's accuracy are 0.9706 and 0.9572, respectively. Overall, the proposed method can provide technical support for the accurate extraction of water body information, which is of great significance for the scientific management of water resources.

*Corresponding author: e-mail: xuwx@fio.org.cn
https://doi.org/10.18494/SAM4064

ISSN 0914-4935
https://myukk.org/

1. Introduction

Water serves as an important resource related to human survival and economic development.[1–4] Whether water is treated as an environmental factor, as a resource, or as a cause of flood disasters, the monitoring and investigation of the nature of water bodies have great significance in the use of natural resources;[5,6] in land use planning, in the development and protection of the environment; and in flood protection and mitigation.[7,8] Remote sensing satellite observations can effectively overcome the limitations that may be encountered in ground mapping, with the graphics of the landscape recorded numerically and processed by computers.[9–11] Remote sensing satellite images cover the entire earth with high-resolution and multiple phases; can accurately record rivers, lakes, coastlines, tidal conditions, and related ground information; and allow scientists to determine the range of a water body quickly and accurately.[12–18] Remote sensing is cheaper than field-survey-based methods, and remotely sensed images provide many economic and social benefits.[19,20]

Since the 1970s, scientists have conducted a considerable amount of research on the extraction of boundaries between water bodies and other ground-based objects.[21,22] From the earliest attempts at edge detection and threshold segmentation to the application of deep learning, methods of extracting water body information have been continuously developing over time.[23,24] The methods used to extract water body information from remote sensing imagery can be divided into three categories: the single-band threshold method, the inter-spectral-relationship-based method, and the water-index-based method.[19,25–28] The single-band threshold method was an early commonly used method. When using a single band of a remote sensing image, the reflectivity of water significantly differs from that of other features, and the water body information can be automatically extracted by setting a threshold. The process of extracting water bodies using the single-band threshold method is relatively simple, and the effects of extracting local water body information are clearly visible. Nevertheless, dense vegetation, mountain shadows, and the water spectrum cannot always be correctly distinguished, and small water bodies cannot be extracted using this method.[29,30] The inter-spectral-relationship-based method extracts water bodies by searching for the difference between the characteristics of the spectral curve of water and other features. This method can extract water bodies as well as distinguish water from shadows, making it suitable for the extraction of water bodies in mountain plateaus.[19,31] This method can also extract the wider part of lakes, larger rivers, and smaller rivers on plains, but a phenomenon known as staggered buildings can create problems. However, a threshold can be used to determine the conditions for the extraction of water bodies from small rivers and those from large urban areas.[32,33] In addition to buildings, this method is also affected by clouds. The water-index-based method is performed by processing the normalized difference in specific wavelength between ground-based objects to highlight water body information in remote sensing images.[3,34,35] The method is very precise, has wide applicability, is simple to operate, and is currently the most widely used and developed method.[36] It can effectively eliminate shadow pixels and improve the accuracy of shadow extraction or of other dark surface areas; however, the reflective surfaces of urban areas, such as ice, snow, and reflective roofs, may be accidentally classified as water.[37,38]

Because the traditional methods discussed above are affected by floating matter, suspended matter, and dissolved matter, it is difficult to extract water bodies with high precision from a wide range of remote sensing images with a complex geographical environment. Toward solving the above problems, we propose a new method of extracting water body information that considers the wetness of ground-based objects. This method is based on the superiority of the tasseled cap transformation (TCT) used in representing the water content of ground-based objects and is combined with threshold value selection by the Otsu method and post-processing supported by mathematical morphology.

2. Methodology

The overall workflow of the proposed method for extracting water body information from remote sensing images is shown in Fig. 1, which can be divided into five steps: (a) pre-processing, (b) TCT, (c) the initial extraction of water body information, (d) the final extraction of water body information, and (e) accuracy assessment.

2.1 Pre-processing

The pre-processing of remote sensing images makes them easily identifiable and interpretable for a particular application. As pre-processing, the digital numbers (DN) in the pixel gray values without physical meaning were converted to top of atmosphere (TOA) reflectance with a clear physical meaning via calibration parameters.

2.2 TCT of Landsat 8 OLI TOA reflectance data

The TCT, also known as the Kauth–Thomas transformation, was first reported in 1976. It uses the maximum segment size data to study the growth of crops and vegetation, with four bands used in the analysis of the maximum segment size.[39–41] In a 4D space, the spectral data points of vegetation are regularly distributed, forming a hatlike shape, giving the TCT its name.[42,43]

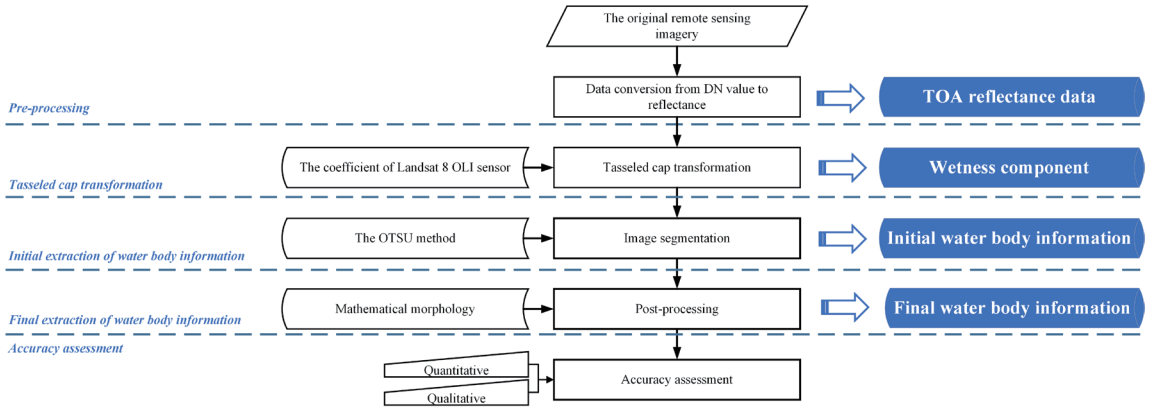

Fig. 1. (Color online) Flowchart of the proposed method.

The TCT has been widely used in remote sensing. It can compress multi-spectral data into a few bands that can be directly linked to physical scene characteristics that are easily understood.[42-44] However, the TCT is sensor-dependent and affected by seasonal changes, and its availability varies with the geographic location.[44,45] Table 1 shows the TCT coefficients of reflectance data for Landsat 8 OLI TOA.[44,46] Band 1 (0.43−0.45 μm) and band 9 (1.36−1.38 μm) of Landsat 8 OLI were not used in the derivation of the TCT coefficients because they are used to detect aerosol and cirrus and provide very little information on land use and land cover.[46]

For satellite remote sensing imagery, a TCT can compress a multi-spectral image into a sum of a set of components, each of which corresponds to a weighted index. The weighted index can reflect each pixel in the original multi-spectral image. The TCT is as follows:[43]

$$y = cx + a, \tag{1}$$

where y is the component in the multi-spectral space after the transformation, x is the Landsat 8 OLI TOA reflectance data, c is the transformation coefficient for Landsat 8 OLI sensors, which is related to the sensors onboard a satellite, and a is a constant used to avoid negative values.

2.3 Initial extraction of water body information based on Otsu method

2.3.1 Selection of threshold value based on Otsu method from wetness component

The Otsu method is a nonparametric and unsupervised method of automatic threshold selection for image segmentation, which usually has a clear border and a uniform internal spectrum.[47,48] In the Otsu method, the threshold k is selected from a gray level histogram ([1, 2, …, L]) to extract objects (C_0) from their background (C_1). All gray level histograms are assessed to select the optimal threshold to maximize the between-class variance.[49] The discriminant criterion (between-class variance) is[47]

$$\sigma^2 = \omega_0(\mu_0 - \mu_T)^2 + \omega_1(\mu_1 - \mu_T)^2, \tag{2}$$

where μ_0, μ_1, and μ_T are the means of class C_0, class C_1, and the original image, and ω_0 and ω_1 are the probabilities of the occurrences of class C_0 and C_1, respectively.

According to the basic principle of the TCT, objects with a high water content, such as rivers, lakes, and oceans, have bright colors, while objects with a low water content, such as buildings,

Table 1
TCT coefficients for Landsat 8 OLI TOA reflectance data.

Band TCT		Band 2 (Blue)	Band 3 (Green)	Band 4 (Red)	Band 5 (NIR)	Band 6 (SWIR 1)	Band 7 (SWIR 2)
Landsat 8	Brightness	0.3029	0.2786	0.4733	0.5599	0.5080	0.1872
	Greenness	−0.2941	−0.2430	−0.5424	0.7276	0.0713	−0.1608
	Wetness	0.1511	0.1973	0.3283	0.3407	−0.7117	−0.4559
	Yellowness	−0.8239	0.0849	0.4396	−0.0580	0.2013	−0.2773

roads, and vegetation, have dark colors. Once the appropriate threshold is selected, a binary image of water can be generated with water assigned a value of 1 and other objects assigned a value of 0, allowing the easy identification of water.

2.3.2 Extraction of initial water body information

The initial water body information was extracted with the formula

$$I_{water} = \begin{cases} 1, & I_{wetness} \geq T_{wetness} \\ 0, & other \end{cases}, \tag{3}$$

where I_{water} is the initial water body information, $I_{wetness}$ is the wetness component after the TCT, and $T_{wetness}$ is the threshold value selected from the wetness component using the Otsu method.

2.4 Final extraction of water body information based on mathematical morphology

The initial water body information involves both the ocean and high-water-content objects such as lakes and rivers. Ships can create holes in initial water body information, and the fact that different objects have the same spectrum leads to some misextraction, which is represented by small plaques. To determine the water body information more accurately, the water bodies surrounded by land (e.g., lakes and rivers) must be post-processed. Considering the differences between lake, river, hole, and misextracted water body information, the mathematical morphology of the initial water body information was used as a tool.

Mathematical morphology is a mathematical tool for image analysis according to morphology.[50,51] As a branch of image interpretation, mathematical morphology was established on the basis of the integral geometry work of Metheron and Serra at Mines Paris Tech, France, in 1964.[52,53] Its basic idea is to use certain structuring elements to measure and extract the corresponding shapes or objects in images to realize visual interpretation and target recognition.[54,55] This method has been widely used in image processing, pattern recognition, and computer vision.[56,57] There are four basic operations in mathematical morphology analysis: erosion, dilation, opening, and closing. Using the external filtering function, dilation can fill the smaller (compared with the size of structuring elements) gaps in images and smooth an object's outline.[58,59] Using the internal filtering function, erosion can eliminate the small fragments in an image and shrink the image.[60–62] Opening can smooth the image, eliminating tiny objects at the edge such as "burrs," or remove the isolated pixels or blocks in an image. Closing has the effect of image filtering, filling up small holes and gaps in an image and filtering nearby objects with a smoothed boundary. These four basic operations can be combined in different ways to generate new operations for morphology analysis.

In this study, we used opening and closing with circular structuring elements for post-processing and obtaining final water body information. According to the basic principle of mathematical morphology, the opening operation removes the misextracted plaques caused by

different objects having the same spectrum, and closing can fill up the holes caused by ships. The method provided the final water body information with high accuracy, avoiding any changes to the original boundaries of the water.

2.5 Accuracy assessment

The accuracy was assessed qualitatively and quantitatively.[63,64] By definition, qualitative evaluation is the assessment of an image produced by visual observation with the support of feature knowledge.[56,65,66] Quantitative evaluation is the assessment of an image using statistical parameters and is generally based on two factors: non-positional and positional accuracies.[56,67] We mainly conducted qualitative evaluation on two factors: location and shape. For the positional accuracy, we calculated the producer's accuracy (PA), user's accuracy (UA), errors of omission (OE), and errors of commission (CE) from the extraction and reference results. For the non-positional accuracy, we calculated the lengths of the coastline in the resulting images and compared them with the length of the real coastline.

The PA is the accuracy of a map from the viewpoint of the mapmaker (the producer).[42,43,56] It indicates how often the physical features on the ground are correctly shown on the classified map or the probability that a certain area on the ground is classified as a given land cover. The UA is the accuracy from the viewpoint of the map user (not the mapmaker). The UA reflects how often the features on a map are actually present on the ground and is referred to as the reliability. The equations for the PA and UA are

$$\begin{cases} \eta & \dfrac{o' \cap o}{o} \\ \eta & \dfrac{o' \cap o}{o'} \end{cases}, \tag{4}$$

where η_1 and η_2 are the PA and UA, and o and o' are the reference data obtained by visual interpretation for a type of surface feature and the data extracted for that type of surface feature, respectively.

Errors of omission refer to the reference sites omitted from the correct class in the classified map.[42,43,56] The errors of omission and commission complement the PA and UA, respectively. The equations for these errors are

$$\begin{cases} \eta_3 = 1 - \eta_1 \\ \eta_4 = 1 - \eta_2 \end{cases}, \tag{5}$$

where η_3 and η_4 are the errors of omission and commission, and η_1 and η_2 are the PA and UA calculated using Eq. (4), respectively.

3. Study Area and Data

3.1 Study area

Hangzhou Bay was selected as the study area to verify the validity and applicability of the proposed method. Hangzhou Bay is located in the northeast of Zhejiang Province, China, where the Qiantang River flows into the East China Sea. It is one of the world's strongest tidal estuaries due to its trumpet shape (Fig. 2).[68,69] Hangzhou Bay is an important part of the Yangtze River Delta owing to its geographical location, dense population, concentrated cities, and developed industry.[70,71] Since China's reform and opening up, the Hangzhou Bay area has witnessed rapid social and economic developments. It is one of the fastest growing regions in China and has brought together a large number of people and economic activities. Hangzhou Bay coastal wetland is one of the eight coastal salt marshes in China and has rich biodiversity.[71-74] Therefore, it is of great significance to extract water body information as an environmental factor for the spatial planning and sustainable development of Hangzhou Bay.

3.2 Data

Landsat 8 OLI images with a spatial resolution of 30 m were used in this study. Beginning in 1972, the Landsat series of satellites has provided the longest continuous record of satellite-based observations.[75–77] As such, Landsat is an invaluable resource for monitoring global changes and a primary source of medium-spatial-resolution earth observations used in decision-making.[77–79] In this study, taking into consideration the imaging time, weather conditions, and cloud cover, we obtained Landsat 8 OLI satellite images of the study area on February 27, 2022.

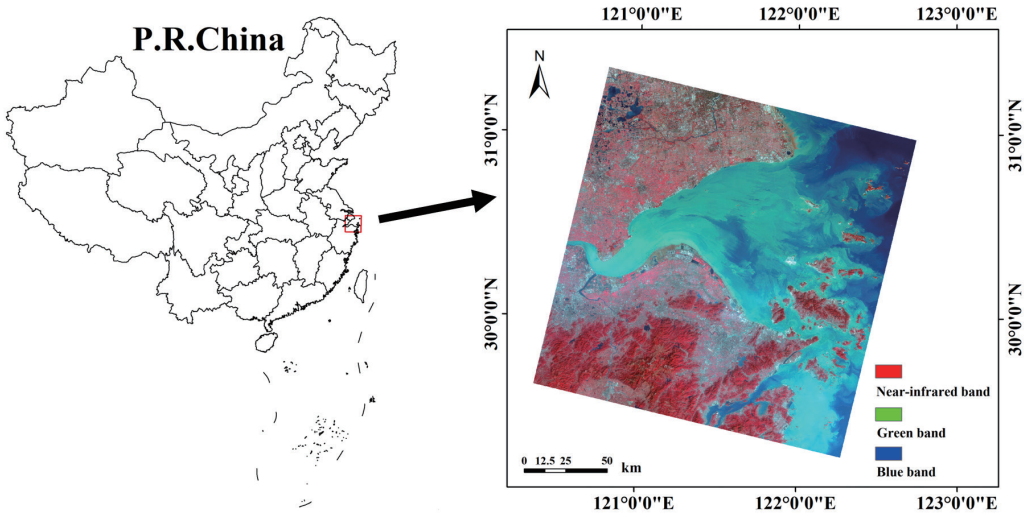

(a) (b)

Fig. 2. (Color online) (a) Geographical location and (b) Landsat 8 OLI image of coverage area of Hangzhou Bay, China. The Landsat 8 OLI image rank band is composed of near-IR, red, and green bands.

4. Results and Analysis

4.1 Water body information extraction from remote sensing images

A TCT was performed on the Landsat 8 OLI TOA reflectance data to obtain four components, brightness, greenness, wetness, and yellowness, using the coefficients in Table 1. The components after the TCT are shown in Fig. 3.

As shown in Fig. 3, the water body shows distribution characteristics different from those of vegetation (including dry fields), human-made features (including roads, residential land, and industrial land), and shadows (mainly mountain and building shadows). Rivers, lakes, and ocean have higher wetness values than other ground objects. The distinction between water and other ground objects in the wetness component is greater than that in the other components.

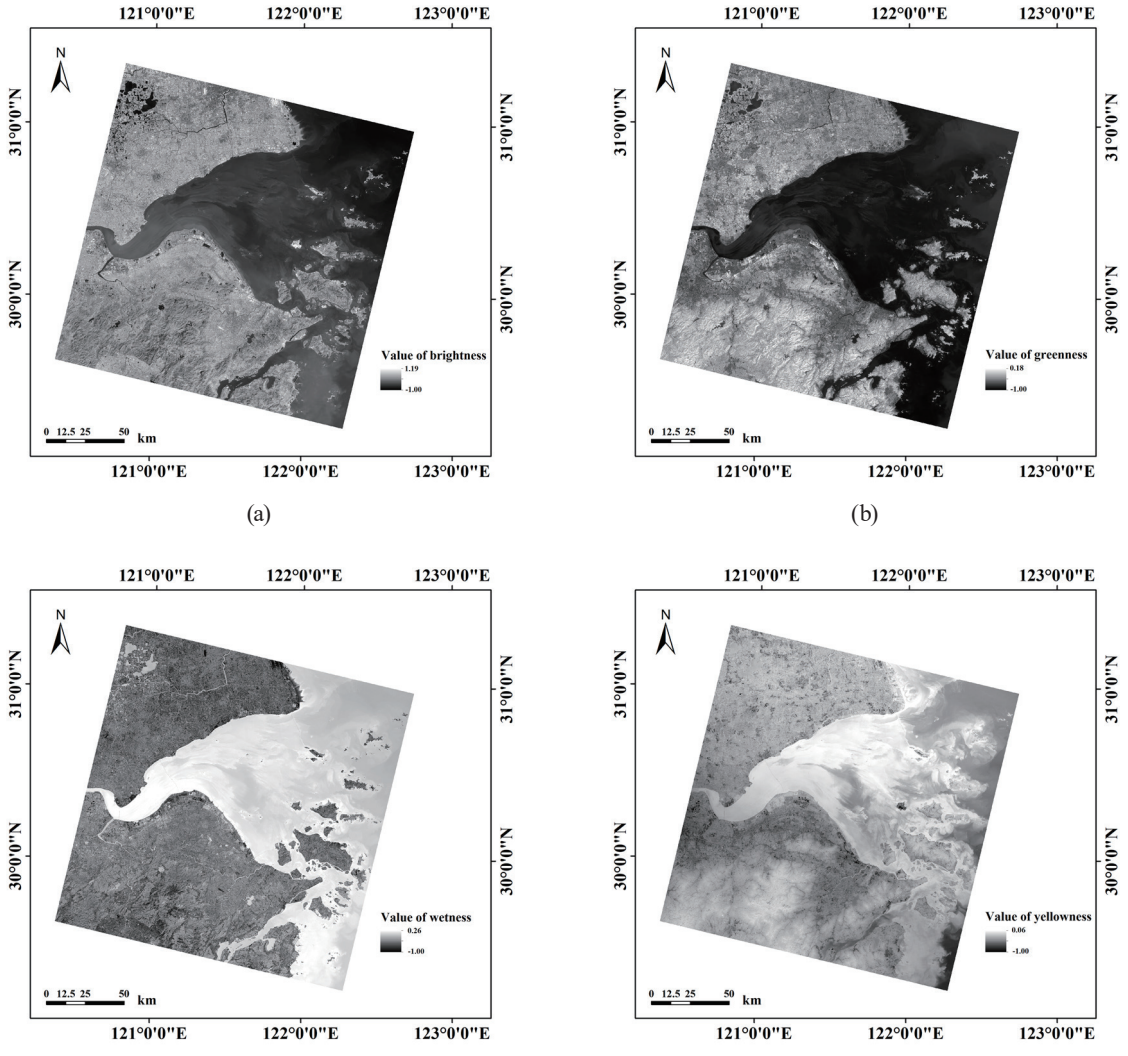

Fig. 3. TCT components. (a) Brightness component, (b) greenness component, (c) wetness component, and (d) yellowness component.

The wetness component was selected for segmentation and to extract initial water body information using the Otsu method. Post-processing was then carried out using mathematical morphology to obtain the final water body information.

The extraction results are shown in Fig. 4.

As shown in Fig. 4, by visually observing the difference between the extraction results and the original remote sensing image, information on water bodies such as rivers, lakes, and ocean was extracted accurately. The results have clear boundaries and accurate locations, and can effectively remove the effects of dense vegetation, suspended sediment, and ships floating on water.

4.2 Accuracy assessment

Accuracy assessment is an important part of information extraction from remote sensing imagery.[16] The boundaries of water bodies were obtained by visual interpretation from high-resolution imagery, and the PA, UA, OE, and CE were calculated on the basis of visual interpretation and the extracted results. The water bodies were obtained by the proposed method and compared with the results obtained by four traditional methods, a near-IR (NIR) band-based method, a normalized difference vegetation index (NDVI)-based method, a normalized difference water index (NDWI)-based method, and a modified normalized difference water index (MNDWI)-based method, to perform a quantitative evaluation of the results (Fig. 5).

Table 2 shows that both the PA and UA of the proposed method are higher than 0.95, and that the OE and CE are lower than 0.05; these values are superior to those obtained by the traditional methods. This indicates that the water body information extracted using the proposed method is consistent with the visual interpretation results and that the proposed method considering the wetness of ground-based objects is reliable and accurate.

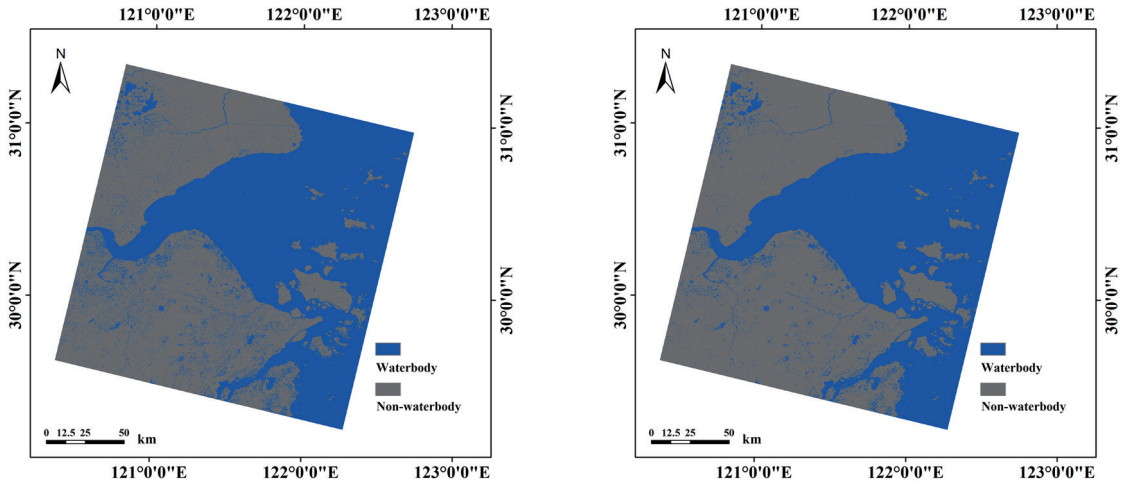

Fig. 4. (Color online) Water body information extracted using the proposed method. (a) Initial and (b) final water body information.

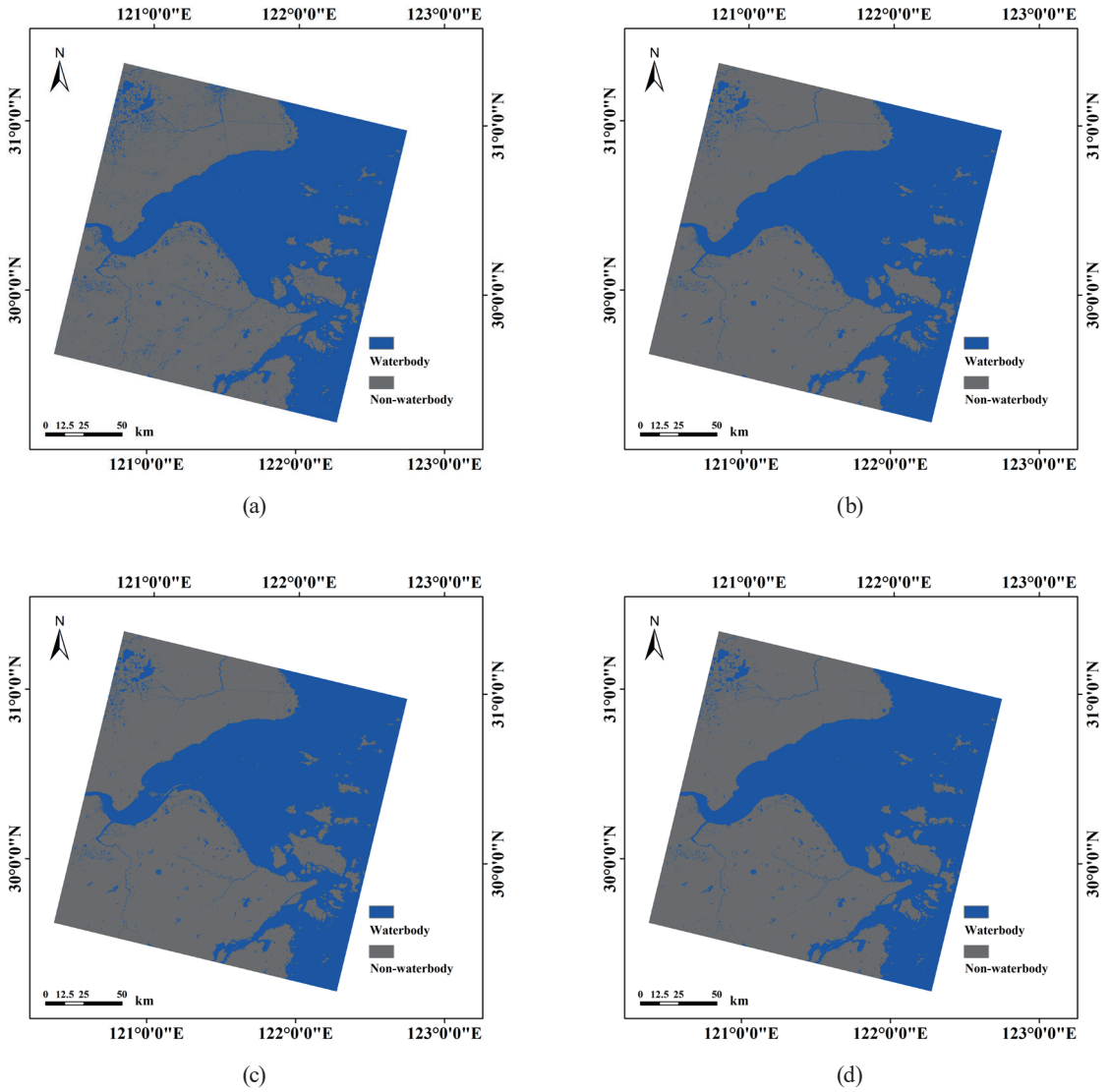

Fig. 5. (Color online) Water body information extracted using traditional methods. (a) NIR band-based, (b) NDVI-based, (c) NDWI-based, and (d) NDWI-based methods.

Table 2
Quantitative evaluation of extracted water body information using different methods.

Method	Formula and threshold value	PA	UA	OE	CE
Proposed method	$I_{wetness} > 0.0320$	0.9706	0.9572	0.0294	0.0428
NIR band-based method	$\rho_{NIR} < 0.0972$	0.8003	0.7922	0.1997	0.2078
NDVI-based method	$(\rho_{NIR} - \rho_{red})/(\rho_{NIR} + \rho_{red}) < 0$	0.8308	0.8235	0.1692	0.1765
NDWI-based method	$(\rho_{green} - \rho_{NIR})/(\rho_{green} + \rho_{NIR}) > 0.0888$	0.8909	0.8491	0.1091	0.1509
MNDWI-based method	$(\rho_{green} - \rho_{NIR})/(\rho_{green} + \rho_{NIR}) > 0.3596$	0.9157	0.8782	0.0843	0.1218

Note: ρ is the reflectance of remote sensing imagery; *red*, *green*, *NIR*, and *MIR* are red, green, NIR, and mid-IR bands, respectively; $I_{wetness}$ is the wetness component obtained by the TCT.

5. Discussion and Conclusions

The components obtained by the TCT are associated with the water content of ground-based objects. In this study, we developed a method of extracting water body information from remote sensing imagery by considering the wetness of ground-based objects to reduce the effects of complex geographical environments with, for example, floating matter, suspended matter, and dissolved matter. After pre-processing the remote sensing image, the TCT, the initial extraction of water body information using the threshold value selected by the Otsu method, and the final extraction of water body information supported by mathematical morphology, we extracted the water body information accurately. An experiment using a Landsat 8 OLI remote sensing image was carried out in Hangzhou Bay, China, to demonstrate and validate this method. Our qualitative and quantitative evaluations verified that the proposed method is accurate, valid, and practical.

The proposed method has high precision and is simple to execute. However, a remaining problem is that the mixed pixels caused the boundaries of the water body information extracted from the remote sensing imagery to be inconsistent with their actual boundaries in the real world. Therefore, the development of a mixed-pixel decomposition method to extract the boundaries of water body information more accurately is required in a follow-up study.

Acknowledgments

We would like to thank the editors and anonymous reviewers for their outstanding comments and suggestions, which greatly helped us to improve the technical quality and presentation of the manuscript. This work was supported by the National Natural Science Foundation of China (Grant No. 42171311), the Open Fund of State Key Laboratory of Remote Sensing Science (Grant No. OFSLRSS202218), and the Training Program of Excellent Master Thesis of Zhejiang Ocean University. We thank Accdon (www.accdon.com) for its linguistic assistance during the preparation of this manuscript.

References

1 N. Wagle, T. D. Acharya, and D. H. Lee: Sens. Mater. **32** (2020) 3879. https://doi.org/10.18494/SAM.2020.2953
2 N. J. Murray, T. A. Worthington, P. Bunting, S. Duce, V. Hagger, C. E. Lovelock, R. Lucas, M. I. Saunders, M. Sheaves, M. Spalding, N. J. Waltham, and M. B. Lyons: Science **376** (2022) 744. https://doi.org/10.1126/science.abm958
3 G. L. Feyisa, H. Meilby, R. Fensholt, and S. R. Proud: Remote Sens. Environ. **140** (2014) 23. https://doi.org/10.1016/j.rse.2013.08.029
4 J. Zhang, C. Zhang, W. Shi, and Y. Fu: J. Hydrol. **568** (2019) 96. https://doi.org/10.1016/j.jhydrol.2018.10.059
5 H. Long, B. Lin, Y. Ou, and Q. Chen: Sci. Total Environ. **690** (2019) 690 1321. https://doi.org/10.1016/j.scitotenv.2019.06.311
6 F. N. Güttler, S. Niculescu, and F. Gohin: Remote Sens. Environ. **132** (2013) 86. https://doi.org/10.1016/j.rse.2013.01.009
7 I. R. Orimoloye, S. P. Mazinyo, A. M. Kalumba, W. Nel, A. I. Adigun, and O. O. Ololade: Earth Sci. Inf. **12** (2020) 12 553. https://doi.org/10.1007/s12145-019-00400-4
8 Z. Du, W. Li, D. Zhou, L. Tian, F. Ling, H. Wang, Y. Gui, and B. Sun: Remote Sens. Lett. **5** (2014) 672. https://doi.org/10.1080/2150704X.2014.960606

9 O. Dubovik, G. L. Schuster, F. Xu, Y. Hu, H. Bösch, J. Landgraf, Z. Li: Front. Remote Sens. **2** (2021) 2 #619818. https://doi.org/10.3389/frsen.2021.619818
10 K. Ostad-Ali-Askar, R. Su, and L. Liu: J. Water Clim. Change **9** (2018) 239. https://doi.org/10.2166/wcc.2018.999
11 C. Chen, J. Liang, F. Xie, Z. Hu, W. Sun, G. Yang, J. Yu, L. Chen, L. H. Wang, L. Y. Wang, H. Chen, X. He, and Z. Zhang: Int. J. Appl. Earth Obs. Geoinf. **107** (2022) 102711. https://doi.org/10.1016/j.jag.2022.102711
12 M. Jia, Z. Wang, D. Mao, C. Ren, C. Wang, and Y. Wang: Remote Sens. Environ. **255** (2021) 112285. https://doi.org/10.1016/j.rse.2021.112285
13 W. R. Becker, T. B. Ló, J. A. Johann, and E. Mercante: Remote Sens. Appl.: Soc. Environ. **21** (2021) 100459. https://doi.org/10.1016/j.rsase.2020.100459
14 A. H. Chughtai, H. Abbasi, and I. R. Karas: Remote Sens. Appl.: Soc. Environ. **22** (2021) 100482. https://doi.org/10.1016/j.rsase.2021.100482
15 P. B. Holden, A. J. Rebelo, and M. G. New: Remote Sens. Appl.: Soc. Environ. **21** (2021) 100448. https://doi.org/10.1016/j.rsase.2020.100448
16 Z. H. Zou, C. Chen, Z. S. Liu, Z. L. Zhang, J. T. Liang, H. X. Chen, and L. Y. Wang: Remote Sens. **14** (2022) 4001. https://doi.org/10.3390/rs14164001
17 G. Yang, K. Huang, W. Sun, X. Meng, D. Mao, and Y. Ge: ISPRS J. Photogramm. Remote Sens. **189** (2022) 236. https://doi.org/10.1016/j.isprsjprs.2022.05.003
18 L. Wang, C. Chen, F. Xie, Z. Hu, Z. Zhang, H. Chen, X. He, and Y. Chu: Int. J. Appl. Earth Obs. Geoinf. **105** (2021) 102616. https://doi.org/10.1016/j.jag.2021.102616
19 C. Chen, H. Chen, J. Liang, W. Huang, W. Xu, B. Li, and J. Wang: Remote Sens. **14** (2022) 3001. https://doi.org/10.3390/rs14133001
20 Z. Duan and W. G. M. Bastiaanssen: Remote Sens. Environ. **134** (2013) 403. https://doi.org/10.1016/j.rse.2013.03.010
21 Y. Wang, Z. Li, C. Zeng, G. S. Xia, and H. Shen: IEEE J. Sel. Top. Appl. Earth Obs. Remote Sens. **13** (2020) 769. https://doi.org/10.1109/JSTARS.2020.2971783
22 D. Li, B. Wu, B. Chen, Y. Xue, and Y. Zhang: J. Tsinghua Univ. (Sci. Technol.) **60** (2020) 147. http://jst.tsinghuajournals.com/EN/10.16511/j.cnki.qhdxxb.2019.22.038
23 A. Fisher, N. Flood, and T. Danaher: Remote Sens. Environ. **175** (2016) 167. https://doi.org/10.1016/j.rse.2015.12.055
24 X. Zhao, P. Wang, C. Chen, T. Jiang, Z. Yu, and B. Guo: Int. J. Remote Sens. **38** (2017) 1404. https://doi.org/10.1080/01431161.2016.1278284
25 H. Y. Liao and T. H. Wen: Int. J. Appl. Earth Obs. Geoinf. **85** (2020) 102003. https://doi.org/10.1016/j.jag.2019.102003
26 J. Lira: Int. J. Remote Sens. **27** (2006) 4015. https://doi.org/10.1080/01431160600702384
27 O. E. Malahlela: Int. J. Remote Sens. **37** (2016) 4574. https://doi.org/10.1080/01431161.2016.1217441
28 X. Lyu, Y. Fang, B. Tong, X. Li, and T. Zeng: Remote Sens. **14** (2022) 4983. https://doi.org/10.3390/rs14194983
29 J. Prošek, K. Gdulová, V. Barták, J. Vojar, M. Solský, D. Rocchini, and V. Moudrý: Int. J. Appl. Earth Obs. Geoinf. **92** (2020) 102181. https://doi.org/10.1016/j.jag.2020.102181
30 X. Wei, W. Xu, K. Bao, W. Hou, J. Su, H. Li, and Z. Miao: Remote Sens. **12** (2020) 3875. https://doi.org/10.3390/rs12233875
31 W. Feng, H. Sui, W. Huang, C. Xu, and K. An: IEEE Geosci. Remote Sens. Lett. **16** (2018) 618. https://doi.org/10.1109/LGRS.2018.2879492
32 L. Li, Z. Yan, Q. Shen, G. Cheng, L. Gao, and B. Zhang: Remote Sens. **11** (2019) 1162. https://doi.org/10.3390/rs11101162
33 L. P. Almeida and R. Almar: J. Mar. Sci. Eng. **8** (2020) 391. https://doi.org/10.3390/jmse8060391
34 S. K. McFeeters: Int. J. Remote Sens. **17** (1996) 1425. https://doi.org/10.1080/01431169608948714
35 H. Xu: Int. J. Remote Sens. **27** (2006) 3025. https://doi.org/10.1080/01431160600589179
36 H. Yue, Y. Li, J. Qian, and Y. Liu: Int. J. Remote Sens. **41** (2020) 7311. https://doi.org/10.1080/01431161.2020.1755740
37 X. Li, F. Ling, X. Cai, Y. Ge, X. Li, Z. Yin, C. Sheng, X. Jia, and Y. Du: Int. J. Appl. Earth Obs. Geoinf. **103** (2021) 102470. https://doi.org/10.1016/j.jag.2021.102470
38 H. Singh, R. D. Garg, and H. C. Karnatak: Earth Sci. Inf. **12** (2020) 307. https://doi.org/10.1007/s12145-019-00378-z
39 E. P. Crist: Remote Sens. Environ. **17** (1985) 301. https://doi.org/10.1016/0034-4257(85)90102-6
40 E. P. Crist and R. C. Cicone: IEEE Trans. Geosci. Remote Sens. GE-**22** (1984) 256. https://doi.org/10.1109/TGRS.1984.350619

41 E. P. Crist and R. C. Cicone: Photogramm. Eng. Remote Sens. **50** (1984) 343. https://ntrs.nasa.gov/citations/19840046937
42 C. Chen, J. Fu, S. Zhang, and X. Zhao: Estuarine Coastal Shelf Sci. **217** (2019) 281. https://doi.org/10.1016/j.ecss.2018.10.021
43 C. Chen, J. Bu, Y. Zhang, Y. Zhuang, Y. Chu, J. Hu, and B. Guo: Adv. Space Res. **64** (2019) 1780. https://doi.org/10.1016/j.asr.2019.07.032
44 Y. Zhai, D. P. Roy, V. S. Martins, H. K. Zhang, L. Yan, and Z. Li: Remote Sens. Environ. **274** (2022) 112992. https://doi.org/10.1016/j.rse.2022.112992
45 Q. Liu, G. Liu, C. Huang, and C. Xie: Int. J. Remote Sens. **36** (2015) 417. https://doi.org/10.1080/01431161.2014.995274
46 M. H. A. Baig, L. Zhang, T. Shuai, and Q. Tong: Remote Sens. Lett. **5** (2014) 423. https://doi.org/10.1080/2150704X.2014.915434
47 N. Otsu: IEEE Trans. Syst. Man Cybern. **9** (1979) 62. https://www.sid.ir/paper/606513/en
48 X. Xu, S. Xu, L. Jin, and E. Song: Pattern Recognit. Lett. **32** (2011) 956. https://doi.org/10.1016/j.patrec.2011.01.021
49 S. Pare, H. Mittal, M. Sajid, J. C. Bansal, A. Saxena, T. Jan, W. Pedrycz, and M. Prasad: Remote Sens. **13** (2021) 4604. https://doi.org/10.3390/rs13224604
50 C. A. Rishikeshan and H. Ramesh: ISPRS J. Photogramm. Remote Sens. **146** (2018) 11. https://doi.org/10.1016/j.isprsjprs.2018.08.014
51 J. Balado, P. Van Oosterom, L. Díaz-Vilarino, and M. Meijers: ISPRS J. Photogramm. Remote Sens. **168** (2020) 208. https://doi.org/10.1016/j.isprsjprs.2020.08.011
52 C. Chen, X. He, Z. Liu, W. Sun, H. Dong, and Y. Chu: Sci. Rep. **10** (2020) 12721. https://doi.org/10.1038/s41598-020-69716-2
53 R. Prabhu, B. Parvathavarthini, and A. R. Alaguraja: J. Appl. Remote Sens. **15** (2021) 014515. https://doi.org/10.1117/1.JRS.15.014515
54 M. Kakooei and Y. Baleghi: Earth Sci. Inf. **13** (2020) 459. https://doi.org/10.1007/s12145-020-00449-6
55 J. M. Fitton, A. F. Rennie, J. D. Hansom, and F. M. Muir: Remote Sens. Appl.: Soc. Environ. **22** (2021) 100499. https://doi.org/10.1016/j.rsase.2021.100499
56 C. Chen, L. Wang, Z. Zhang, C. Lu, H. Chen, and J. Chen: J. Appl. Remote Sens. **16** (2022) 012006. https://doi.org/10.1117/1.JRS.16.012006
57 H. Chen, C. Chen, Z. Zhang, C. Lu, L. Wang, X. He, Y. Chu, and J. Chen: Ocean Coastal Manage. **213** (2021) 105842. https://doi.org/10.1016/j.ocecoaman.2021.105842
58 A. El Jazouli, A. Barakat, R. Khellouk, J. Rais, and M. El Baghdadi: Remote Sens. Appl.: Soc. Environ. **13** (2019) 361. https://doi.org/10.1016/j.rsase.2018.12.004
59 Z. Liu, L. Wang, and B. Li: Front. Ecol. Evol. (2022). https://doi.org/10.3389/fevo.2022.918756
60 A. Spinosa, A. Ziemba, A. Saponieri, L. Damiani, and G. El Serafy: J. Mar. Sci. Eng. **9** (2021) 575. https://doi.org/10.3390/jmse9060575
61 S. N. MohanRajan, A. Loganathan, P. Manoharan: Environ. Sci. Pollut. Res. **27** (2020) 29900. https://doi.org/10.1007/s11356-020-09091-7
62 D. S. Maia, M. T. Pham, and S. Lefèvre: IEEE J. Sel. Top. Appl. Earth Obs. Remote Sens. **15** (2022) 2574. https://doi.org/10.1109/JSTARS.2022.3153110
63 K. Huang, G. Yang, Y. Yuan, W. Sun, X. Meng, and Y. Ge: Sci. Remote Sens. **5** (2022) 100040. https://doi.org/10.1016/j.srs.2022.100040
64 H. Su, Y. Peng, C. Xu, A. Feng, and T. Liu: J. Appl. Remote Sens. **15** (2021) 018504. https://doi.org/10.1117/1.JRS.15.018504
65 X. Yang, Z. Zhu, S. Qiu, K. D. Kroeger, Z. Zhu, and S. Covington: Remote Sens. Environ. **276** (2022) 113047. https://doi.org/10.1016/j.rse.2022.113047
66 W. Feng, H. Sui, W. Huang, C. Xu, and K. An: IEEE Geosci. Remote Sens. Lett. **16** (2018) 618. https://doi.org/10.1109/LGRS.2018.2879492
67 H. W. Khalid, R. M. Z. Khalil, and M. A. Qureshi: Egypt. J. Remote Sens. Space. Sci. **24** (2021) 619. https://doi.org/10.1016/j.ejrs.2021.09.003
68 Y. Xu, X. He, Y. Bai, D. Wang, Q. Zhu, and X. Ding: Remote Sens. **13** (2021) 4267. https://doi.org/10.3390/rs13214267
69 L. Chu, Y. Zou, D. Masiliūnas, T. Blaschke, and J. Verbesselt: GISci. Remote Sens. **58** (2021) 199. https://doi.org/10.1080/15481603.2020.1868212
70 D. Xu, Z. Cai, D. Xu, W. Lin, J. Gao, and L. Li: Land **11** (2022) 867. https://doi.org/10.3390/land11060867

71 L. Wang, C. Chen, Z. Zhang, W. Gan, J. Yu, and H. Chen: J. Appl. Remote Sens. **16** (2021) 12010. https://doi.org/10.1117/1.JRS.16.012010
72 T. Kutser, J. Hedley, C. Giardino, C. Roelfsema, and V.E. Brando: Remote Sens. Environ. **240** (2020) 111619. https://doi.org/10.1016/j.rse.2019.111619
73 X. L. Liu, N. Adil, and X. L. Ma: Sens. Mater. **33** (2021) 4561. https://doi.org/10.18494/SAM.2021.3441
74 L. Zhang, H. Zhang, Y. Niu, and W. Han: Remote Sens. **11** (2019) 605. https://doi.org/10.3390/rs11060605
75 G. Pugliano, U. Robustelli, D. Di Luccio, L. Mucerino, G. Benassai, and R. Montella: J. Mar. Sci. Eng. **7** (2019) 137. https://doi.org/10.3390/jmse7050137
76 M. K. Gumma, P. S. Thenkabail, P. G. Teluguntla, A. Oliphant, J. Xiong, C. Giri, V. Pyla, S. Dixit, and A. M. Whitbread: GISci. Remote Sens. **57** (2020) 302. https://doi.org/10.1080/15481603.2019.1690780
77 Y. F. He, C. Chen, B. Li, and Z. L. Zhang: Remote Sens. Appl.: Soc. Environ. **28** (2022) 100824. https://doi.org/10.1016/j.rsase.2022.100824
78 E. F. Berra, R. Gaulton, and S. Barr: Remote Sens. Environ. **223** (2019) 229. https://doi.org/10.1016/j.rse.2019.01.010
79 Z. Lv, G. Li, Z. Jin, J. A. Benediktsson, and G.M. Foody: IEEE Trans. Geosci. Remote Sens. **59** (2021) 139. https://doi.org/10.1109/TGRS.2020.2996064